HHS Public Access

Author manuscript

Stat Atlases Comput Models Heart. Author manuscript; available in PMC 2022 September 01.

Published in final edited form as:

Stat Atlases Comput Models Heart. 2022 September ; 13131: 132–140.

doi:10.1007/978-3-030-93722-5_15

Statistical shape analysis of the tricuspid valve in hypoplastic left heart sydrome

Jared Vicory[1], **Christian Herz**[2], **David Allemang**[2], **Hannah H. Nam**[2], **Alana Cianciulli**[2], **Chad Vigil**[2], **Ye Han**[1], **Andras Lasso**[3], **Matthew A. Jolley**[2], **Beatriz Paniagua**[1]

[1]Kitware Inc, North Carolina, USA

[2]Children's Hospital of Philadelphia, Philadelphia, PA, 02115, USA

[3]Queen's University, Ontario, Canada

Abstract

Hypoplastic left heart syndrome (HLHS) is a congenital heart disease characterized by incomplete development of the left heart. Children with HLHS undergo a series of operations which result in the tricuspid valve (TV) becoming the only functional atrioventricular valve. Some of those patients develop tricuspid regurgitation which is associated with heart failure and death and necessitates further surgical intervention. Repair of the regurgitant TV, and understanding the connections between structure and function of this valve remains extremely challenging. Adult cardiac populations have used 3D echocardiography (3DE) combined with computational modeling to better understand cardiac conditions affecting the TV. However, these structure-function analyses rely on simplistic point-based techniques that do not capture the leaflet surface in detail, nor do they allow robust comparison of shapes across groups. We propose using statistical shape modeling and analysis of the TV using Spherical Harmonic Representation Point Distribution Models (SPHARM-PDM) in order to generate a reproducible representation, which in turn enables high dimensional low sample size statistical analysis techniques such as principal component analysis and distance weighted discrimination. Our initial results suggest that visualization of the differences in regurgitant vs. non-regurgitant valves can precisely locate populational structural differences as well as how an individual regurgitant valve differs from the mean shape of functional valves. We believe that these results will support the creation of modern image-based modeling tools, and ultimately increase the understanding of the relationship between valve structure and function needed to inform and improve surgical planning in HLHS.

Keywords

Statistical shape modeling; statistical shape analysis; hypoplastic left heart syndrome; pediatric cardiac imaging; 3D echocardiography

1 Introduction

Hypoplastic left heart syndrome (HLHS) is a form of congenital heart disease characterized by incomplete development of the left heart, yielding a left ventricle that is incapable of supporting the systemic circulation. HLHS affects over 1,000 live born infants in the US per year and would be uniformly fatal without intervention [5]. Staged surgical

treatment allows children with HLHS to survive and flourish, but the right ventricle (RV) remains the sole functioning ventricle and the tricuspid valve (TV) the sole functioning atrioventricular valve. Tricuspid regurgitation (TR) is highly associated with heart failure and death and necessitates surgical intervention in almost 30% of HLHS patients [7]. Defining the mechanisms of TR is difficult, with both 2D echocardiography (2DE) and surgical inspection having significant limitations [13]. We instead analyze the structure of the TV in 3D echocardiography (3DE) images with the goal of detecting and quantifying TR.

Gross metrics that attempt to model the geometry of a structure, such as diameter, area, or volume, have been used as intuitive measurements in medical imaging studies. Previous work has investigated the use of such metrics to quantitatively detect the presence and severity of TR. For the TV, these metrics include annular area [3, 11], septolateral diameter [3, 4, 11], bending angle [8], anterior leaflet prolapse [4], and anterior papillary muscle location [3, 11]. While some of these measures are restricted to a certain region or leaflet of the TV, they are still summarizing these regions rather than modeling them directly and so can not always reflect localized structural changes.

In contrast, shape is a proven biomarker that is more robust and, in many cases, more clinically relevant than traditional 2D or 3D-based metrics. Statistical Shape Modeling (SSM) can be used to quantitatively characterize shape and produce models that represent the average shape of a population as well as the principal modes of variation. Further, these modeling techniques can precisely quantify the location and magnitude of differences between two populations (e.g. regurgitant vs. non-regurgitant valves) and can do so with fewer assumptions and less bias than traditional approaches.

In this paper we describe a semi-automatic pipeline for creating 3D models of TV leaflet surface geometry suitable for statistical analysis and demonstrate its usefulness in several experiments. The ultimate goal of this modeling is to compare the shape of the TV in patients with moderate or greater TR to those with mild or lower to correlate structure to TV dysfunction.

2 Materials

2.1 Subjects

Acquisition of transthoracic 3DE images of the TV is part of the standard clinical echo lab protocol for HLHS at the Children’s Hospital of Philadelphia (CHOP). An institutional database was used to retrospectively identify patients with HLHS with a Fontan circulation in whom 3DE of the TV had been previously performed. Exclusion criteria included presence of significant stitch artifact and inability to delineate the TV. This study was performed according to a protocol approved by the CHOP Institutional Review Board (IRB). We have 100 3DE scans with age range 2.14 years to 30.64 years, with an average of 10.36 years. Images were acquired using sector narrowed Full Volume or 3D Zoom mode with a wide FOV. EKG gated acquisitions were obtained when patient cooperation allowed. Transthoracic X7 or X5 probes were used with the Philips IE33 and EPIQ 7 ultrasound systems.

3 Methods

3.1 Image Segmentation and Model Creation

Images were exported to Philips DICOM, converted to cartesian DICOM in QLAB, and imported into 3D Slicer [1] using the SlicerHeart [2, 3] Philips DICOM converter. A single mid-systolic frame was chosen for static 3D modeling of the TV. TV segmentation was performed using the 3D Slicer Segments module.

3.2 Modeling the TV

We propose to represent TV geometry via point distribution models (PDMs) of each leaflet. We generate these models by first parametrizing the segmentations using spherical harmonics [6] and then use icosahedron subdivision to obtain densely-sampled boundary PDMs using the SPHARM-PDM software package available in SlicerSALT [15]. When applied to modeling the TV, this modeling technique does not require user input other than providing the number of structures in the model (three leaflets for a tricuspid valve).

While SPHARM-PDM can often produce high-quality correspondence with no post-processing, this is not the case for the TV. To bring the SPHARM-PDM models into correspondence, we adapt the approach of Lyu [9] and use specific anatomical landmarks to guide correspondence improvement. For each leaflet, we map three manually identified landmarks (the two commisures and the valve center) on the SPHARM mesh back to their location on the underlying spherical parameterization. Then, choosing one case as a template, we rotate the spherical parameterization of the other cases to minimize the distances between the sets of landmark locations in parameter space. We then remesh each leaflet using its rotated parameterization to obtain PDMs with the same geometry but with vertices reindexed to have better correspondence. Quality control of the correspondences for each leaflet type is performed using the color-coded spherical parameterization. Equally colored areas represent equal corresponding areas. Figure 2 shows the result of this procedure for a subset of 40 septal leaflets.

Finally, models of the TV were built by merging the SPHARM-PDM models of the septal, anterior and posterior leaflets into a multi-object PDM of the entire TV which can be analyzed using the methods described in the next sections.

Before statistical shape analysis, we pre-process the population of SPHARM-PDM correspondent models by aligning and scaling it using standard Procrustes analysis. Second, we replaced the Procrustes computed scaling with body surface area (BSA) for normalization. We normalize shape geometry of the TV using BSA instead of by scale because that metric has a been used in cardiology before to predict physiologic outcomes such as flow rates.

3.3 Principal Component Analysis

We use Principal Component Analysis, a method for computing an efficient parameterization of the variability of linear data (in this case the 3-dimensional correspondent points contained in our spharm models), to build low dimensional statistical

shape spaces for each one of the TR/severity subgroups as well as the healthy group. Thanks to our interactive tools, we can explore the generated PCA space and to evaluate the quality of the generated models.

3.4 Distance Weighted Discrimination

DWD is a binary classification method designed to address shortcomings with support vector machine (SVM) performance when applied to high-dimension, low-sample-size (HDLSS) data [10, 16] by considering the effects of all data on the separating hyper-plane rather than just a limited set of support vectors. Here, we apply DWD to classify the PDMs of each TV by regurgitation severity into trivial/mild or moderate/severe severity. Like SVM, DWD performs classification by computing the distance of each sample to a separating hyperplane, with samples laying on the same side of the hyperplane being classified together.

4 Results

4.1 Shape modeling

During our initial experiments with SPHARM-PDM we realized that the heuristic methods applied to ensure the spherical topology of the segmentation were significantly (as large as 0.8mm) changing the thin structures of the individual TV leaflets. Due to this fact, we decided to bypass this step and directly compute surface meshes corresponding and the spherical parametrizations on the original segmentation. Following the correspondence optimization process described in section 3.2, high-quality models were successfully generated for all three leaflets in all 100 TV images.

4.2 Principal Component Analysis

We use principal component analysis (PCA) to compute the mean and major modes of variation of the population of TV models and explore the existing phenotypes in our population. Figure 3 shows the mean and four most significant modes of variation for our sample. The first mode is essentially pure scaling, that is present after rescaling all geometry by BSA, while the next three show scaling of each of the individual leaflets. While these modes intuitively make sense they do not turn out to be particularly relevant for correlating structural changes with functional ones. Instead, we investigate the use of DWD for this purpose.

4.3 Distance Weighted Discrimination

Thanks to DWD we were able to examine the effect of different regurgitation levels in TV geometry. In order to do this, we group the existing four categories in two groups, i.e. trivial/mild cases and moderate/severe, because the boundaries between the four categories can be somewhat arbitrary.

Figure 4 shows the effects of different scale normalization schemes in classification results. For each subject we compute the distance to the separating hyperplane and use kernel density estimation to fit probability distributions to each severity group. The discrimination power between different regurgitation levels is greatly reduced by not normalizing the

correspondent point based models or by just normalizing using the gross scale computed by Procrustes (see Figure 4.a. and 4.b.). Surprisingly normalizing with both gross scale and BSA tend to incorrectly classify valves as Trivial/Mild, indicating that the distance to the hyperplane is not independent of scale or BSA, while the unscaled models show relatively good separation between the classes. Additionally, we see a strong discrimination between trivial and severe groups when scaling using BSA is performed, indicating a correlation between regurgitation degree and TV geometry.

Projecting samples orthogonally to the separating hyperplane, also called the separation direction, is also an excellent visualization tool that relates our functional marker, regurgitation, to valve geometry. In figure 5 we show shapes from both sides of the separating hyperplane as you move from far from the plane on one side through the plane and far to the other side. This shows a clear progression from tenting on the trivial/mild side to billowing on the severe side, consistent with the clinical observation that regurgitant valves tend to have more billow.

5 Discussion

In this paper we introduce a pipeline for semi-automatically creating representations of tricuspid valve leaflet boundaries suitable for statistical analysis using SPHARM-PDM followed by a novel correspondence-optimizing post-processing. We demonstrate the effectiveness of this modeling approach by using statistical shape analysis approaches such as PCA and DWD to examine the difference between valves with trivial or mild regurgitation and those with moderate or severe regurgitation. PCA results are of limited usefulness due to the challenging nature of the problem, natural normal variability within this population, and our normalization strategy, but DWD analysis is able to show clear linkages between the geometry captured between the best separating axis between these two clinical populations and functional variables such as the tenting volume on the whole TV or the individual tenting volume of each individual leaflet, indicating that our representations are able to capture clinically relevant information.

We have identified several paths forward for future work on this problem. Regarding modeling, our current semi-automatic pipeline could be fully automated by developing methods for automatically placing landmarks at the commisures and center of the valve. We are also exploring methods for automatically segmenting the TV from ultrasound, further reducing the manual effort required to get from data acquisition to analysis. We will also continue to refine our analysis pipeline by investigating other clinical variables as well as investigating additional statistical shape analysis approaches. Finally, we will investigate the relationship between the various traditional metrics used to detect TR to changes in shape to determine if these effects can be further localized or if shape analysis can provide additional power than these metrics alone.

We will continue to investigate different normalization approaches because, as our PCA results show, our current approach using BSA is not sufficient for fully separating the relationship between the size of a TV and its shape and may in fact be introducing additional dependence between the two. We will investigate normalizing by other metrics of the TV,

including various transformations of BSA along with more direct measures such as annular diameter. We will also investigate using metrics based on the full heart, such as ventricular length or volume, though these are also problematic due to potential ventricular dilation correlated with TR. We will also investigate using age-specific normalization strategies to attempt to separate normal growth from abnormal annulus dilation which can be associated with TR.

In addition to the SPHARM-PDM boundary models described here, we are also investigating the use of skeletal models [12] for representing and analyzing TVs. Skeletal models have been shown to be powerful representations for statistical shape analysis and due to the thin nature of the TV leaflets we hypothesize that they will be particularly well-suited to this problem.

Acknowledgements

Research reported in this publication was supported by the National Institute of Biomedical Imaging and Bioengineering from the National Institutes of Health under Award Number R01HL153166 as well as the National Institute of Biomedical Imaging and Bioengineering under award number R01EB021391. The content is solely the responsibility of the authors and does not necessarily represent the official views of the National Institutes of Health. The methods presented in this work are distributed as part of SlicerSALT [14], an open-source, free, comprehensive software that will allow biomedical scientists to precisely locate shape changes in their imaging studies, and SlicerHeart [3, 2], a 3DSlicer extension containing tools for cardiac image import (3D/4D ultrasound, CT, MRI), quantification, and implant placement planning and assessment.

References

[1]. Fedorov A et al. “3D Slicer as an image computing platform for the Quantitative Imaging Network”. In: Magnetic resonance imaging 30.9 (Nov. 2012), pp. 1323–1341. issn: 1873–5894. doi: 10.1016/J.MRI.2012.05.001. [PubMed: 22770690]

[2]. Scanlan AB et al. “Comparison of 3D Echocardiogram-Derived 3D Printed Valve Models to Molded Models for Simulated Repair of Pediatric Atrioventricular Valves”. In: Pediatric cardiology 39.3 (Mar. 2018), pp. 538–547. issn: 1432–1971. doi: 10.1007/S00246-017-1785-4. [PubMed: 29181795]

[3]. Nguyen AV et al. “Dynamic Three-Dimensional Geometry of the Tricuspid Valve Annulus in Hypoplastic Left Heart Syndrome with a Fontan Circulation”. In: Journal of the American Society of Echocardiography : official publication of the American Society of Echocardiography 32.5 (May 2019), 655–666.e13. issn: 1097–6795. doi: 10.1016/J.ECHO.2019.01.002. [PubMed: 30826226]

[4]. Bautista-Hernandez Victor et al. “Mechanisms of tricuspid regurgitation in patients with hypoplastic left heart syndrome undergoing tricuspid valvuloplasty”. In: The Journal of thoracic and cardiovascular surgery 148.3 (2014), pp. 832–840. [PubMed: 25129586]

[5]. Gordon BM et al. “Decreasing number of deaths of infants with hypoplastic left heart syndrome”. In: The Journal of pediatrics 153.3 (Sept. 2008), pp. 354–358. issn: 1097–6833. doi: 10.1016/J.JPEDS.2008.03.009. [PubMed: 18534240]

[6]. Brechbühler Ch, Gerig Guido, and Kübler Olaf. “Parametrization of closed surfaces for 3-D shape description”. In: Computer vision and image understanding 61.2 (1995), pp. 154–170.

[7]. Barber G et al. “The significance of tricuspid regurgitation in hypoplastic left-heart syndrome”. In: American heart journal 116.6 Pt 1 (1988), pp. 1563–1567. issn: 0002-8703. doi: 10.1016/0002-8703(88)90744-2. [PubMed: 2461647]

[8]. Kutty Shelby et al. “Tricuspid regurgitation in hypoplastic left heart syndrome: mechanistic insights from 3-dimensional echocardiography and relationship with outcomes”. In: Circulation: Cardiovascular Imaging 7.5 (2014), pp. 765–772. [PubMed: 25073974]

[9]. Lyu Ilwoo et al. “Robust estimation of group-wise cortical correspondence with an application to macaque and human neuroimaging studies”. In: Frontiers in neuroscience 9 (2015), p. 210. [PubMed: 26113807]

[10]. Marron JS, Todd Michael J, and Ahn Jeongyoun. “Distance-Weighted Discrimination”. In: Journal of the American Statistical Association 102.480 (2007), pp. 1267–1271. doi: 10.1198/016214507000001120. eprint: 10.1198/016214507000001120.

[11]. Nii Masaki et al. “Three-dimensional tricuspid annular function provides insight into the mechanisms of tricuspid valve regurgitation in classic hypoplastic left heart syndrome”. In: Journal of the American Society of Echocardiography 19.4 (2006), pp. 391–402. [PubMed: 16581478]

[12]. Pizer Stephen M et al. “Object shape representation via skeletal models (s-reps) and statistical analysis”. In: Riemannian Geometric Statistics in Medical Image Analysis. Elsevier, 2020, pp. 233–271.

[13]. Bharucha T et al. “Right ventricular mechanical dyssynchrony and asymmetric contraction in hypoplastic heart syndrome are associated with tricuspid regurgitation”. In: Journal of the American Society of Echocardiography : official publication of the American Society of Echocardiography 26.10 (Oct. 2013), pp. 1214–1220. issn: 1097–6795. doi: 10.1016/J.ECHO.2013.06.015. [PubMed: 23876994]

[14]. Vicory Jared et al. “SlicerSALT: Shape AnaLysis Toolbox”. In: Shape in Medical Imaging : International Workshop, ShapeMI 2018, held in conjunction with MICCAI 2018, Granada, Spain, September 20, 2018, Proceedings. International Workshop on Shape in Medical Imaging (2018 : Granada, Spain). Vol. 11167. Springer, Cham, Sept. 2018, pp. 65–72. doi: 10.1007/978-3-030-04747-4_6.

[15]. Vicory Jared et al. “Slicersalt: Shape analysis toolbox”. In: International Workshop on Shape in Medical Imaging. Springer. 2018, pp. 65–72.

[16]. Wang Boxiang and Zou Hui. “Another look at distance-weighted discrimination”. In: Journal of the Royal Statistical Society: Series B (Statistical Methodology) 80.1 (2018), pp. 177–198. doi: 10.1111/rssb.12244. eprint: https://rss.onlinelibrary.wiley.com/doi/pdf/10.1111/rssb.12244.

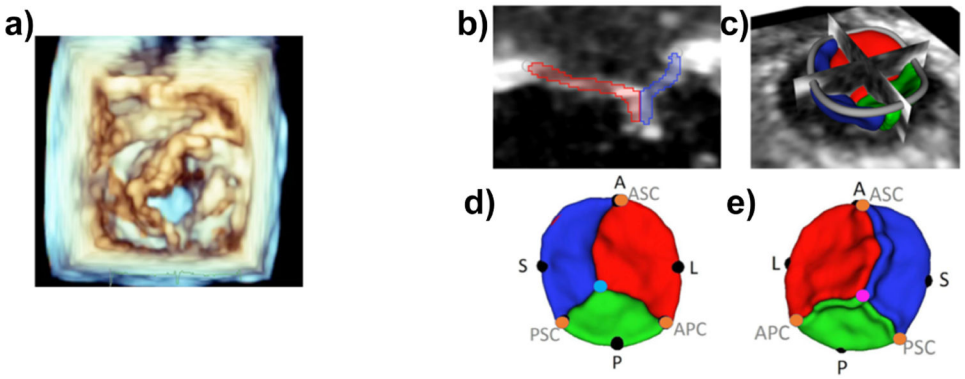

Fig.1:

A. Volume rendering of 3DE (left ventricular view) of TV in patient with HLHS; B and C. Segmentation of TV; D and E. Atrial and ventricular views of valve model with landmark annotations(A = anterior, P = posterior, S = septal, L = lateral, ASC, APC, PSC = commisures)

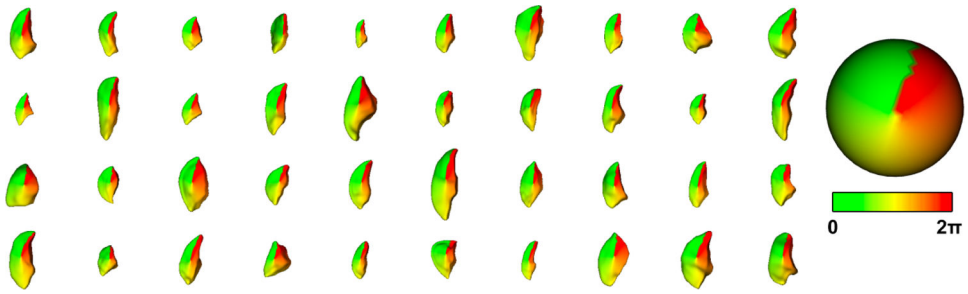

Fig.2:

Visualization of the SPHARM-PDM correspondence using the ϕ-attribute shown on forty randomly selected septal leaflets. Corresponding anatomical locations have similar colors, indicating good correspondence.

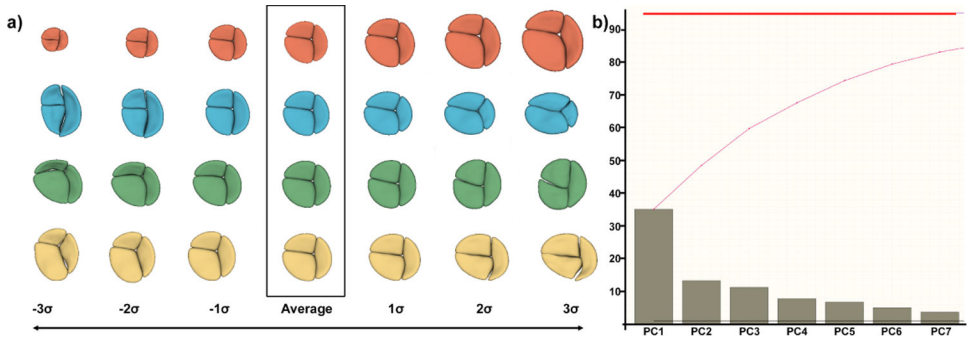

Fig.3:

a) Axes of geometric variation in the TV population. (red) First principal component (PC) showing TV scale, even after normalization. (blue) Second PC capturing sizing on the septal leaflet. (green) Third PC capturing size of the anterior leaflet. (yellow) Fourth PC capturing size of the posterior leaflet. b) Scree plot showing the variability contained in the first seven principal components does not reach 85% of explained variability, indicating a complex problem

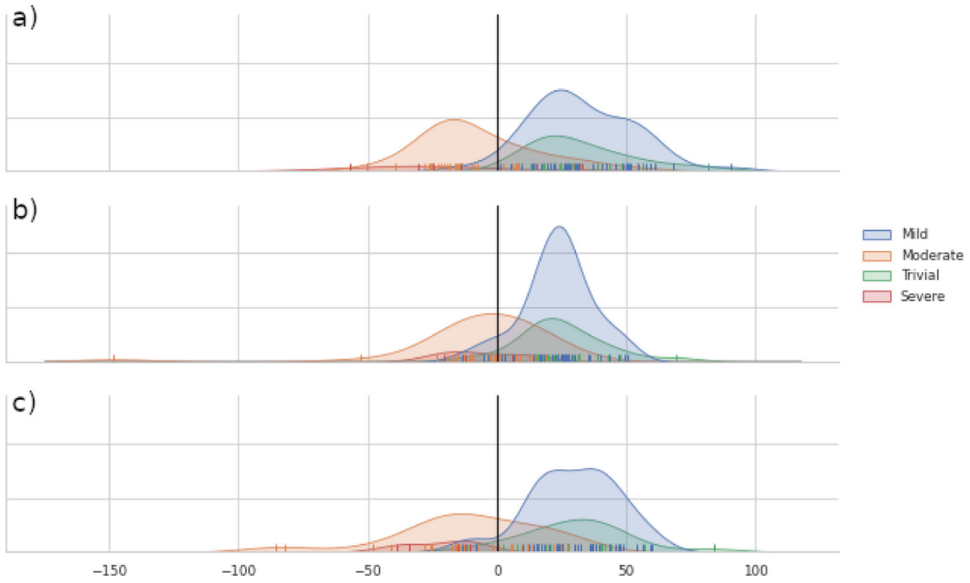

Fig.4:

Kernel density estimate of the signed distance to DWD separating hyperplane for a) No scaling, b) Scaling using BSA, and c) Scaling using gross geometric scale.

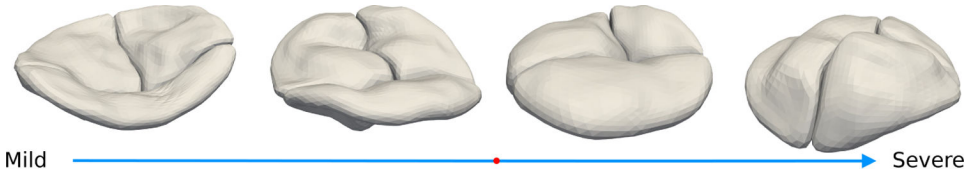

Fig.5:

Example shapes sorted by distance along the DWD separation direction from the trivial/mild side (left) to the moderate/severe side (right). The red dot shows the location of the separating hyperplane. Shapes show more billow as regurgitation gets more severe.